BIOLOGICAL CRYSTALLOGRAPHY

Acta Cryst

D

Volume 71 (2015)

Supporting information for article:

Room-temperature serial crystallography at synchrotron X-ray sources using slowly flowing free-standing high-viscosity microstreams

Sabine Botha, Karol Nass, Thomas R. M. Barends, Wolfgang Kabsch, Beatrice Latz, Florian Dworkowski, Lutz Foucar, Ezequiel Panepucci, Meitian Wang, Robert L. Shoeman, Ilme Schlichting and R. Bruce Doak

S1. Description of the Sample Injector.

The High Viscosity Extrusion (HVE) sample injector employed in these measurements is of the same general design as that developed by Weierstall and colleagues at ASU (Weierstall *et al.*, 2014), but redesigned and fabricated at the Max Planck Institute for Medical Research. Apart from a few stock parts, listed below, the injector was entirely a custom fabrication. The general features can be seen in Supplementary Fig. S1.
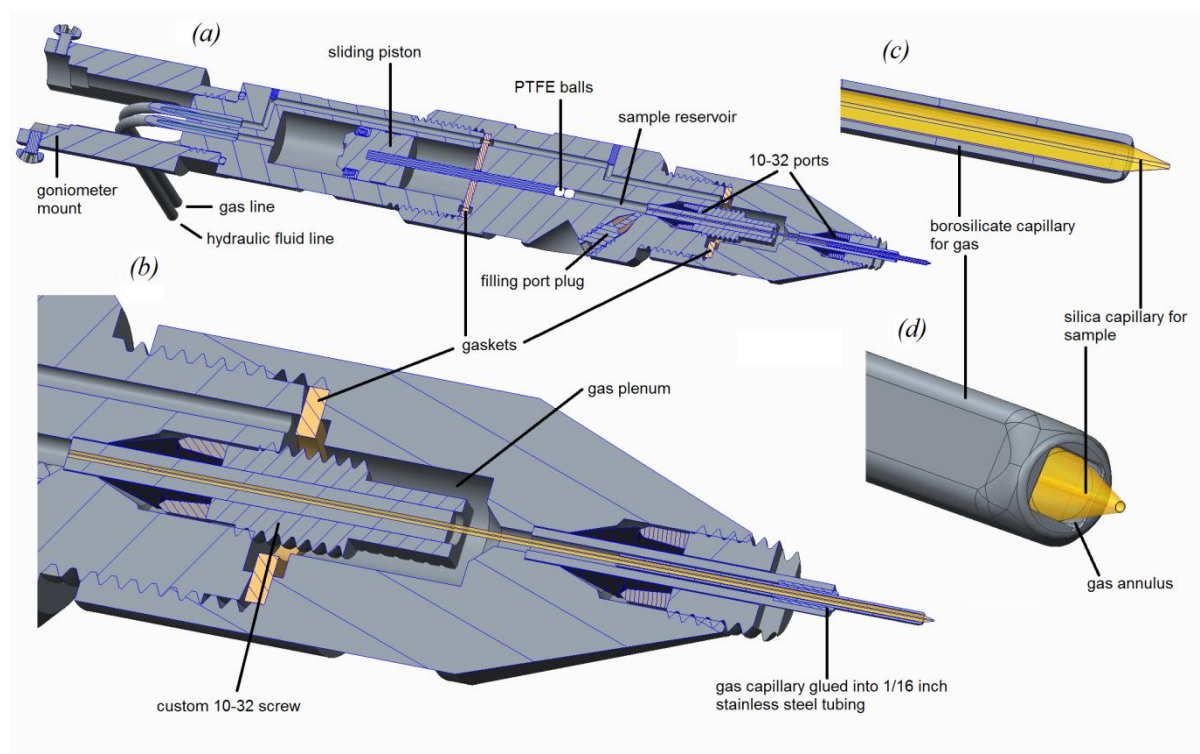

Figure S1 High Viscosity Extrusion (HVE) Injector.

(*a*) Overall cross-sectional view. (*b*) Detailed view of front end of injector. (*c*) Tip region of the injector, showing the coned silica sample capillary centred in the flame-burnished end-aperture of the surrounding sheath of square glass tubing. The high viscosity carrier medium, carrying embedded crystals, extrudes from the bore of this capillary. (*d*). Detailed view of the coned tip of the capillary pressed into the semi-square gas aperture. This geometry positions and centres the capillary tip in the sleeve aperture and also allows gas to flow out through the open corners, preventing curling up of the emerging high viscosity free-stream.

A spring-loaded O-ring (Trelleborg Sealing Solutions, Turcon Variseal M2 Single Acting Spring Energized Seal, PVA000080-T40SD) seals a sliding piston within an 8.00 mm ID cylindrical bore (Figure S1 (*a*)). A 1.35 mm OD rod (McMaster-Carr, High-Speed M2 Tool Steel Hardened Undersized Rod, 2900A218) is rigidly attached via thermal shrink-fit into the piston body. This rod extends into a 1.37 mm ID reservoir, where its lead end contacts two PTFE balls of 1.588 mm diameter (Engineering Laboratories, www.plasticballs.com), which press-fit into the reservoir bore to provide a high-pressure sliding seal. Crystals of interest, embedded into a high viscosity carrier medium, are loaded into the reservoir prior to inserting the PFTE balls. Pressure applied to the rear surface of the piston forces the piston forward and thereby the rod, applying amplified pressure through the PTFE ball seal to the contents of the reservoir bore. The pressure amplification, neglecting sliding wall friction, equals the ratio of the cross-sectional areas of piston to rod, specifically an amplification factor of 34 for the current bore diameters. Assuming no leaks in the injector plumbing, the volumetric flow rate of the extruded stream is smaller than the hydraulic fluid flow by the same ratio of 34. The front end of the sample reservoir terminates in a standard Upchurch 10-32 port (http://www.idex-hs.com/support/upchurch/spd1Eng.aspx) to mount the silica capillary (Molex - Polymicro Technologies, TSP Fused Flexible Silica Capillary Tubing, typically TSP TSP020375 or TSP040375) through which the high viscosity carrier medium, with the embedded crystals of interest is extruded. To withstand the very high pressures that can develop across this fitting, a custom-made 10-32 screw with 3 mm wrench flats (Figure S1 (*b*)) is used to compress a commercial high-pressure ferrule (IDEX Health and Science, Upchurch Scientific, Ultra-High Performance Fingertight Fitting PK-100 Ferrule Set). Still further forwards, a second Upchurch 10-32 port mounts a stainless steel tube (Upchurch Scientific, Stainless Steel Tubing U-115 or alternatively U-101 drilled 0.080 mm diameter, 6-8 mm deep) into which a borosilicate capillary of square cross-section (Friederich and Dimmock, Borosilicate Square Tubing BST-040-10) is epoxied (Figure S1 (*a,b*)). The distal end of the square capillary is ground and flame burnished to yield a semi-square aperture at the capillary tip (Figure S1 (*d*)). This sleeve is mounted concentrically around the silica capillary and carefully positioned such that the conical surface of the capillary comes into light contact with the inside flats of the sleeve aperture. This leaves the capillary tip centred in the semi-square aperture and protruding ca 0.5-1 mm beyond it (Figure S1 (*c,d*)).

In operation, hydraulic fluid and gas are supplied to the injector through two stainless steel tubing lines (Upchurch Scientific, Stainless Steel Tubing U-107) hard-soldered into the rear of the piston section (Figure S1 (*a*)). The hydraulic fluid (to date always simply water) drives the piston forward, applying amplified pressure via the rod and PTFE ball seal to the high viscosity sample solution, which then extrudes out through the central capillary. The incoming gas (generally helium) is ducted through internal cavities within the injector to the region between the two Upchurch ports (Figure S1 (*b*), gas plenum). Here it enters and passes through the annular region between the central capillary

and the outer sleeve, then flows out through the open corner apertures of the "conical-peg-in-a-square-hole." (Figure S1 (*d*)) In contrast to low viscosity gas-focused free streams, the high viscosity extrusion stream is not reduced in diameter by this coaxial gas flow. Nonetheless, the gas flow is crucial to maintaining a straight-line form of the extruded stream, which would otherwise curl up in the fashion of toothpaste squeezed from its tube, sticking to the injector tip instead of extruding in a stable linear stream. The gas flow exerts shear force on the free-stream, resulting in a net axial gas dynamic force on the emerging stream that increases with the length of the extruded segment, until eventually some or all of the extruded segment breaks away and flies off downstream. Flow conditions can often be found under which this rupture occurs several millimetre downstream of the nozzle, allowing a steady, uniform, linear extrusion to be maintained in the region where the X-ray beam intersects the stream, immediately downstream of the nozzle tip as seen in figure 1 of the main text which shows a screen shot prepared using the beam line microscope camera. (Please note: since the original X-ray scale box and labelling on the screen shot is extremely difficult to visualize at the magnification of this image, the scale box was filled with black color and the size labels were removed electronically.) The extruding stream is often observed to form a ball at its apex prior to stream rupture.

As seen in Supplementary Fig. S1 *(a,b)*, the injector consists of a piston section, a sample reservoir section, and a front cap. These separate sections unscrew to provide access to the piston, to the capillary, and for loading the sample reservoir. The connections are sealed by knife-edges that bite into a gasket disk cut from PTFE and a Viton O-ring. Recessed annular cavities adjacent to the O-ring, combined with holes drilled through the gasket, eliminate the need for azimuthal alignment upon screwing these joints together. A custom-made "bubbler" hydration unit can be inserted into the gas supply line, if desired, to saturate the gas with water or other liquids. The injector body was originally constructed to mount within the ASU injector shroud designed by Doak (Weierstall *et al.*, 2012). For the synchrotron measurements described here, a simple conversion part (Figure S1 (*a*)) was fabricated to mount the assembly onto the goniometer of PXII-X10SA, a macromolecular crystallography beamline at the Swiss Light Source (SLS). A detailed view the HVE injector, mounted at PXII-X10SA, looking directly upstream into the oncoming X-ray beam, is given in Supplementary Figure 2.
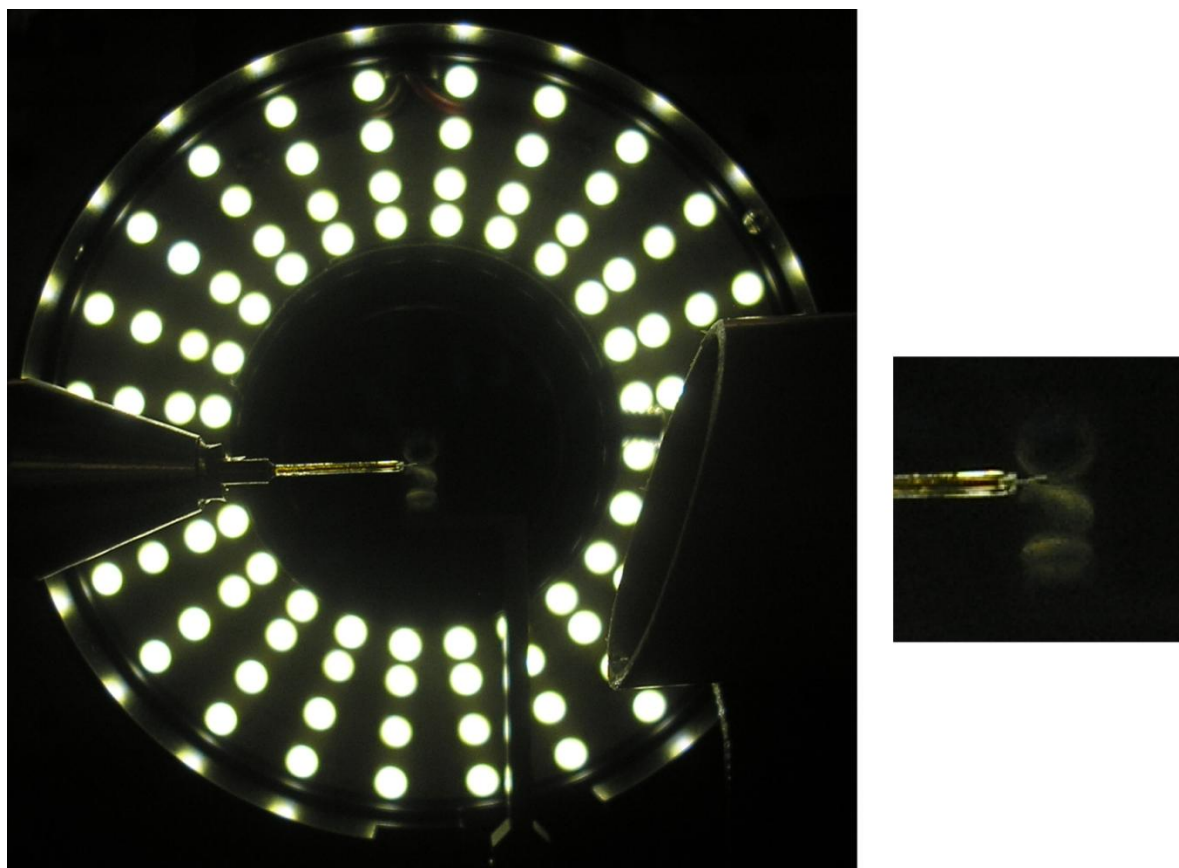
Figure S2 HVE injector in operation.

The view is upstream into the X-ray beam. The tiny thread in the centre of the photograph (enlarged image to right) is a 40 µm diameter sample free-stream extruding from the injector nozzle (left) towards the catcher tube (right). The white LEDs of the ring light illumination system can be seen in the background.

Although much heavier than the sample loop that would normally be mounted on the goniometer, the injector can nonetheless be positioned using the goniometer's x and y drives. Care had to be taken that the gas and liquid supply lines did not exert unwanted forces on the goniometer button. The z motion provides adequate movement along the axis of the injector to align the stream with the X-ray beam. Rotation of the injector by up to several degrees about its long axis is possible even with the stainless steel supply lines, and much further in angle when these were replaced with flexible silica capillaries. Alignment of the high viscosity stream with the X-ray is carried out using the usual beamline control software, as are the experimental measurements, including rotation around the spindle axis if desired.

The HVE injector has been tested with a variety of carrier media including LCP, Vaseline™, MeBiol gels, silicone oils and their mixtures, over a range of dynamic viscosity from about 10^5 to 10^6 centiStokes (cSt). The required hydraulic drive pressure depends strongly on viscosity, capillary inner diameter, and capillary length. For a 40 µm ID capillary of 43 mm length, it varies from about 5 to

400 pounds per square inch gauge (psig) over this viscosity range, implying pressures in the sample reservoir of 170 to 13600 psig. The HPLC pump (Shimadzu Corporation, Solvent Delivery Unit LC-20AD) employed to pressurize the hydraulic fluid can nominally supply up to 6000 psig. The piston system is indispensable, both to separate hydraulic fluid from the sample medium and to restrict the size of the sample reservoir. The usable stroke of the piston is nominally 22.5 mm, corresponding to a sample volume of 33 μl. The flow speed of the extruded free-stream typically ranges from 50 μm/s to several mm/s with e.g. Vaseline™. With a 40 μm ID capillary the corresponding nominal sample consumption is 4 to 300 nl/min, allowing measuring times of 140 to 2 hours with a full sample reservoir. An independent check on sample consumption rate is provided by the HPLC pump, which is run in a flow-rate controlled mode. This pump can nominally be set to flow rates as low as 0.1 μl/min. In a typical HVE experiment it is often set to 0.5 and 7.0 μl/min for the hydraulic fluid, corresponding to a volumetric flow rate in the extruded stream of 15 to 200 nl/min.

Sample is loaded into the injector by unscrewing the injector assembly at the connection between the hydraulic piston section and the front two sections, which can be done without removing the piston section from the goniometer. The piston is pushed to the rear of its 8 mm ID bore. The two PTFE balls are removed from the 0.157 mm sample reservoir, sample is loaded via syringe with a blunt needle into the proximal end of the reservoir, taking care to fill the bore completely and to leave no voids. Two fresh PTFE balls, one after the other, are then carefully pressed into the reservoir bore and then further advanced into the reservoir until sample begins to extrude from the tip of the nozzle. The sample reservoir section is then screwed back into place on the piston section and the hydraulic fluid pressurized until steady extrusion begins. The free-stream extrusion is then centred on the X-ray beam using the XYZ movements under observation with the beamline camera.
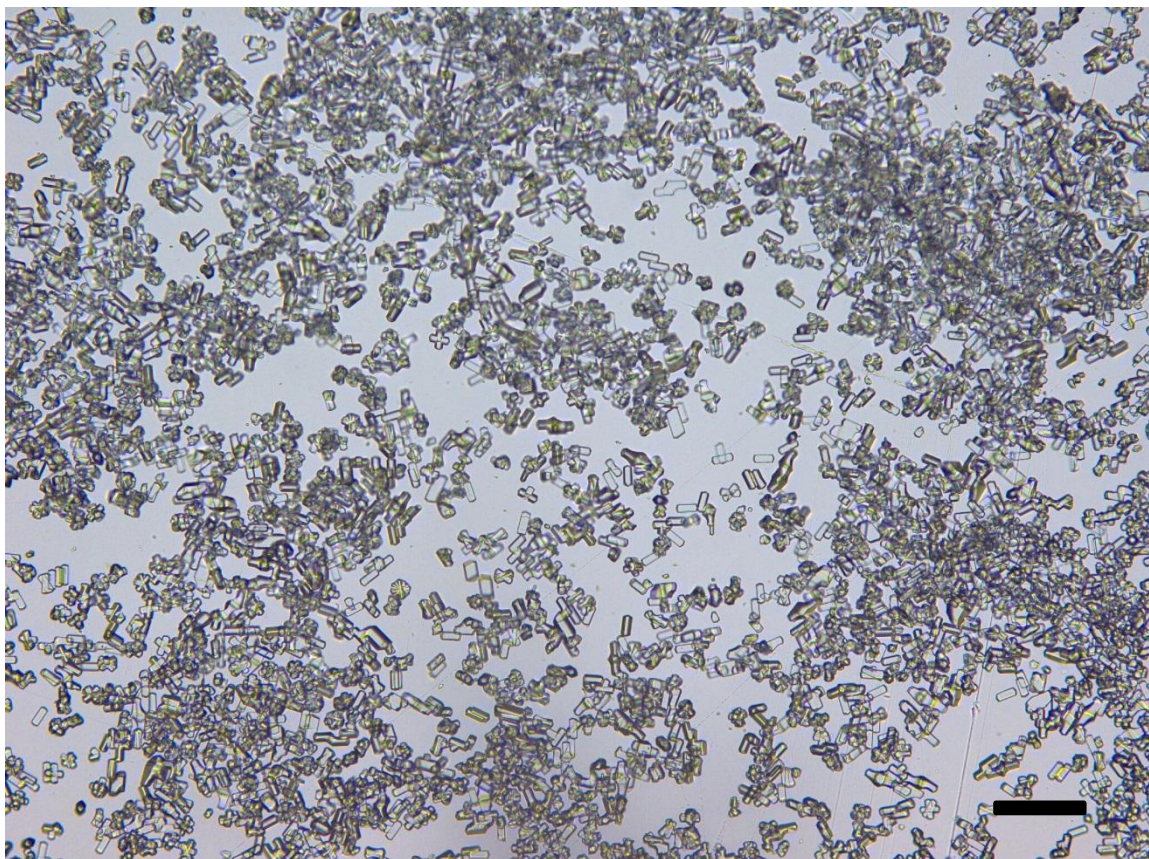
Figure S3 Microcrystals.

Example of hen egg-white lysozyme crystals used for SX experiments. The average size of the crystals is $10 \times 10 \times 30$ μm^3. The scale bar (black) is 100 μm.

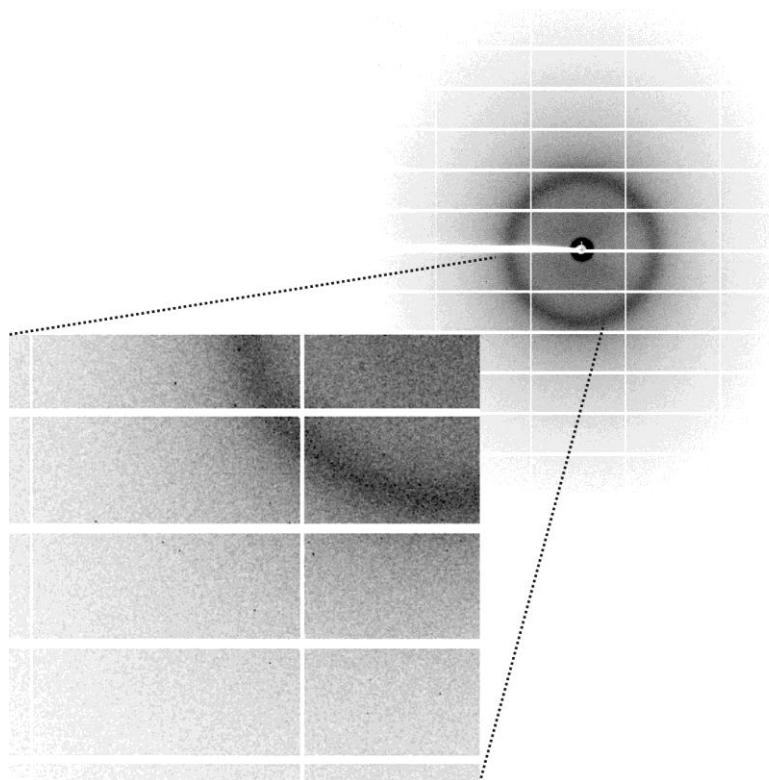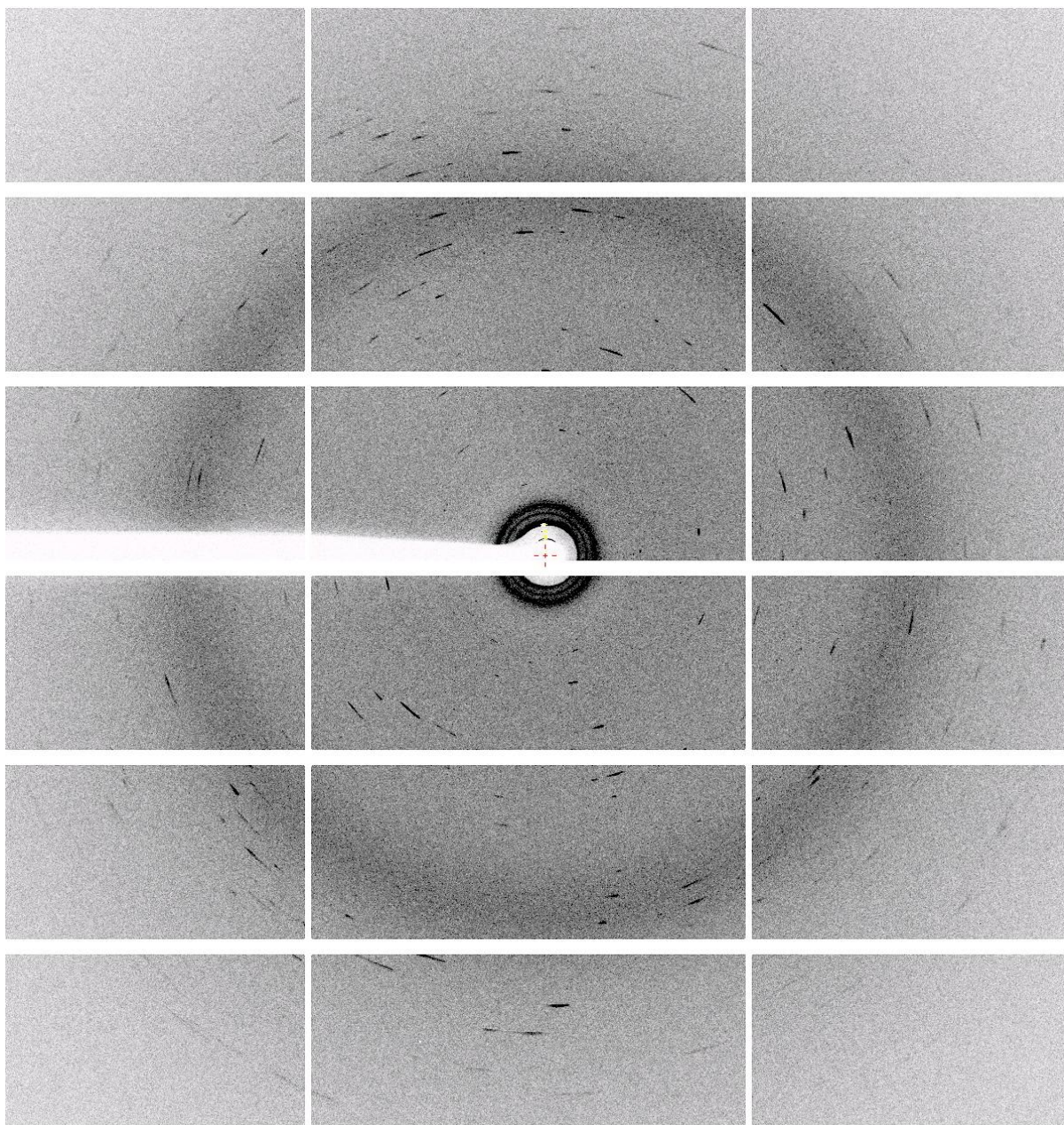**Figure S4** Diffraction pattern from a lysozyme crystal ($10\times10\times30$ µm^3) embedded in monoolein LCP, collected using 1.32 Å wavelength X-rays.

Figure S5 Diffraction pattern of a lysozyme crystal (10 x 10 x 30 um^3), embedded in monoolein LCP, rotating azimuthally around the X-ray beam axis during the 100 ms exposure.
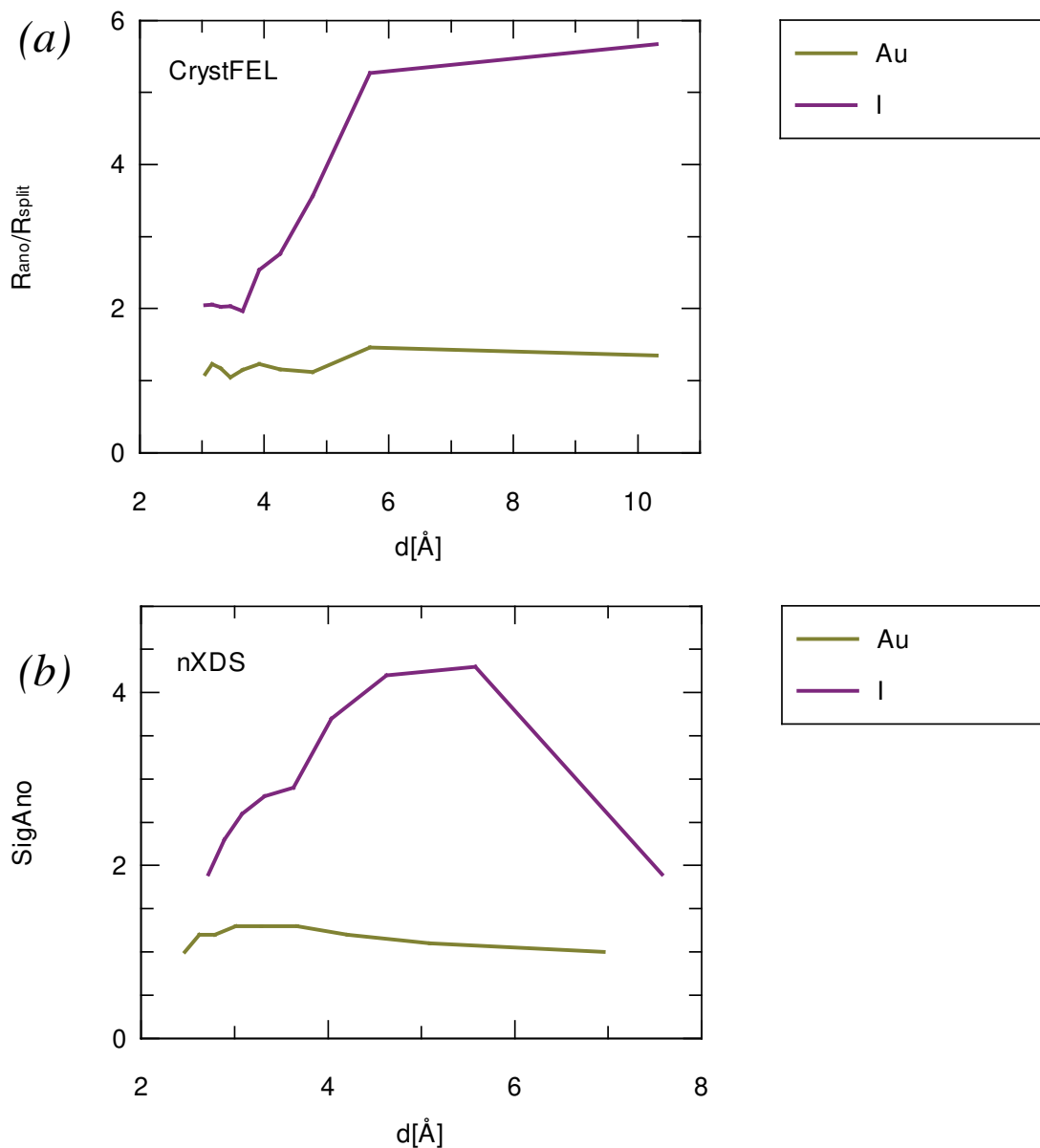
Figure S6 Anomalous signal-to-noise ratios. Since CrystFEL and nXDS determine sigma values differently, a comparison of the statistics produced by the two programs is difficult. We therefore present here R_{ano}/R_{split} (Weiss, 2001, Weiss *et al.*, 2001, Barends *et al.*, 2014) for the CrystFEL data (panel (a)) and SigANO for the nXDS data (b), which are both a measure of the anomalous signal-to-noise ratio.
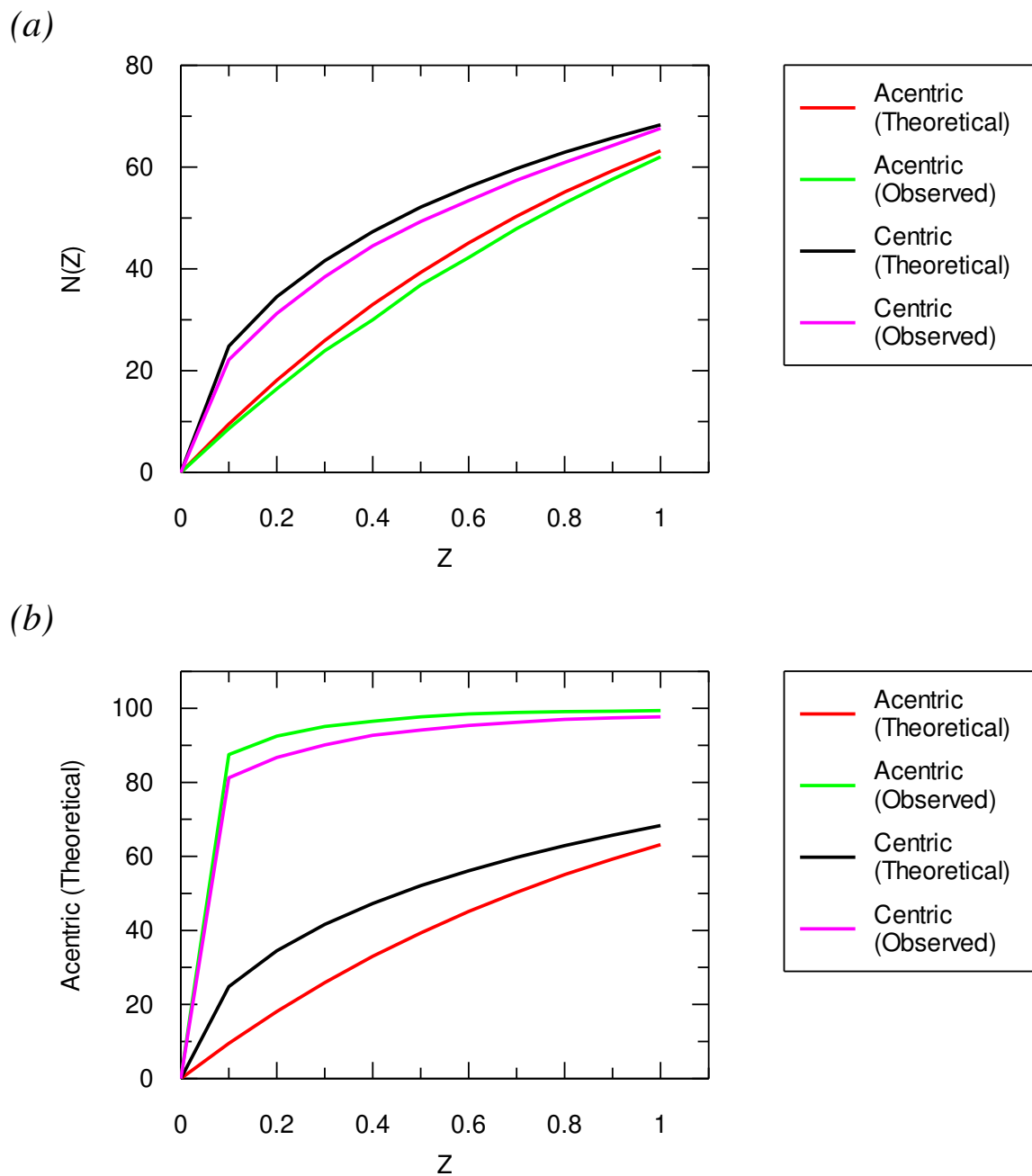
(a)

(b)

Figure S7 Cumulative intensity distributions of the native data processed by (a) nXDS and (b) CrystFEL. Distributions were calculated using TRUNCATE. Weak reflections are overrepresented in the data from CrystFEL.

S2. Vaseline as a carrier medium.

We investigated Vaseline[TM] (petroleum jelly) as an alternative carrier medium. While it results in Debye-Scherrer rings at 4.2 and 3.77 Å spacing (Figure S8) (plus additional weak rings at higher resolution) it has several advantages: (i) it can form thinner streams than LCP at reasonable extrusion pressures, (ii) the viscosity and thus the flowrate can be adjusted by the amount of mother liquor added, unlike LCP that requires a defined mixing ratio, and (iii) its consistence is much silkier than LCP making it more gentle for the embedding of fragile crystals.

To compare the diffuse background scattering caused by Vaseline with that caused by LCP, we selected 10056 diffraction images without Bragg peaks from a run with Vaseline as the carrier medium, and compared the radial average (normalized to the number of images) with that from 2991 Bragg-peak-free images from a run in LCP (Figure S8). In both cases, a 40 μm ID capillary was used for extrusion and the X-ray energy was 8.5 keV.

The images displayed in Fig. S6 b) and c) are a summation of all the diffraction images without Bragg peaks divided by the number of images that were summed.

The angular average and the resolution in panel (a) was calculated by going through all the pixels of the PILATUS diffraction image that are positive, since negative pixel values indicate a gap or a bad pixel. For each pixel the corresponding radius was calculated using the direct beam position in pixels and the pixel size in meter provided by the cbf header:

$$r_m = \sqrt{(i_{Column} - cx_{pix} * pixsizeX_m)^2 + (i_{Row} - cy_{pix} * pixsizeY_m)^2}$$

with r_m being the radius on the detector in meter, i_{Column} and i_{Row} indicating the pixel column and row index numbers, cx_{pix} and cy_{pix} the position of the direct beam in x and y, respectively and $pixsizeX_m$ and $pixsizeY_m$ being the size of the pixels in meter.

The resolution is calculated by

$$R = \frac{1}{\frac{2}{\lambda_A} \sin(\frac{1}{2} \tan^{-1}(\frac{r_m}{d_m}))}$$

with λ_A being the wavelength in Ångström, r_m the calculated radius in meter, and d_m the detector distance in meter.

These calculated values alongside with the pixel value were put into a list. The r_m and R values were then histogrammed using the pixel values as weight for the plot showing the radial average in m and in resolution space, respectively. Subsequently, the individual bins were normalized to the number of values that had been put into each bin. The resulting histogram was plotted. 1000 and 200 bins were used for the radial average and the resolution plot, respectively.
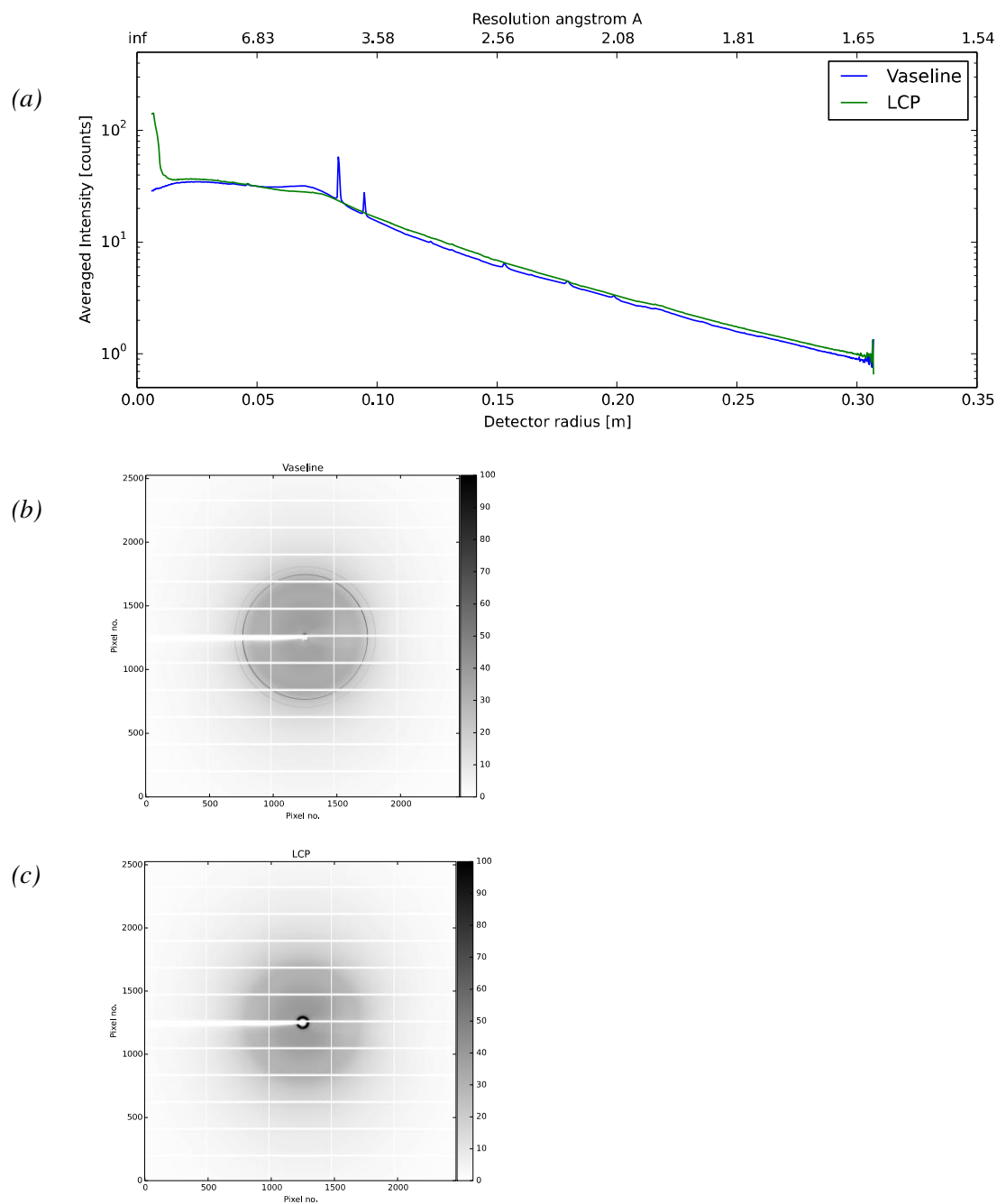
Figure S8 Diffuse scattering from injection media

(a) Radial averages of the background scattering caused by a Vaseline stream (blue) and an LCP stream (green). *(b)* Diffraction image of a Vaseline stream. *(c)* Diffraction image of an LCP stream. Whereas the Vaseline stream has characteristic Debye-Scherrer rings, the LCP stream shows strong diffuse scattering at low resolution.

S3. Comparison of the HVE experiments with the Stellato *et al.* and Boutet *et al.* experiments.

The geometry of our experiment leads to lower X-ray absorption than that of the experiment described by Stellato *et al.* (Stellato *et al.*, 2014). Using the interaction cross-sections tabulated by NIST in their XCOM database for photoelectric effect as well as elastic and inelastic scattering (which can be accessed at http://physics.nist.gov/PhysRefData/Xcom/html/xcom1.html), the total X-ray absorption by the setup and the sample can be estimated.

Assuming for Stellato *et al.* a sandwich of 100 µm of 10% NaCl, 28% PEG and 0.5 M sodium acetate in water between two 10 µm layers of glass (SiO_4), the transmission of 9.8 keV photons can be calculated as ~0.85. In contrast, for the current experiment setup, using the formula $C_{21}H_{40}O_4$ for monoolein (which is 40% of the sample) and using 8% NaCl, 0.1 M Na-acetate, a transmission of 0.97 can be calculated for the HVE injector experiment assuming a 40 µm stream thickness and 9.4 keV photons. For the Boutet experiment (Boutet *et al.*, 2012), assuming a 4 µm stream of 10% NaCl, 1 M Na-acetate at 9.4 keV, the calculated transmission is >0.99. This shows that gas-focussed free-flowing streams have a significant advantage over confined samples in terms of absorption and background.

The native lysozyme crystals ($10 \times 10 \times 30$ µm^3) used in our experiments (9.4 keV photons (1.5×10^{12} photons/s in 10×30 µm^2) absorbed a maximal dose of ~310 kGy/crystal (average diffraction weighted dose ~170 kGy), taking into account the contributions of 8% NaCl mother liquor, and assuming that the crystal was in the beam during the entire exposure time of 0.1 s (calculated by RADDOSE-3D (Zeldin *et al.*, 2013). This is similar to the maximal dose of 0.3 MGy given by Stellato *et al.* who report their crystal size as smaller ($3 \times 3 \times 6$ µm^3), and used a microfocussed beam (2×10^{12} 9.8 keV photons/s in 9×6 µm^2) and fast framing detector (25 Hz instead of 10 Hz as in our case).

Figure S9 Vertical mount of the HVE injector. Using a bracket, the injector can be mounted perpendicular to the spindle axis shown on the left. This has the advantage that gravity provides additional stability to the vertically extruding jet. The collimator can be seen on the right of the extruding stream.
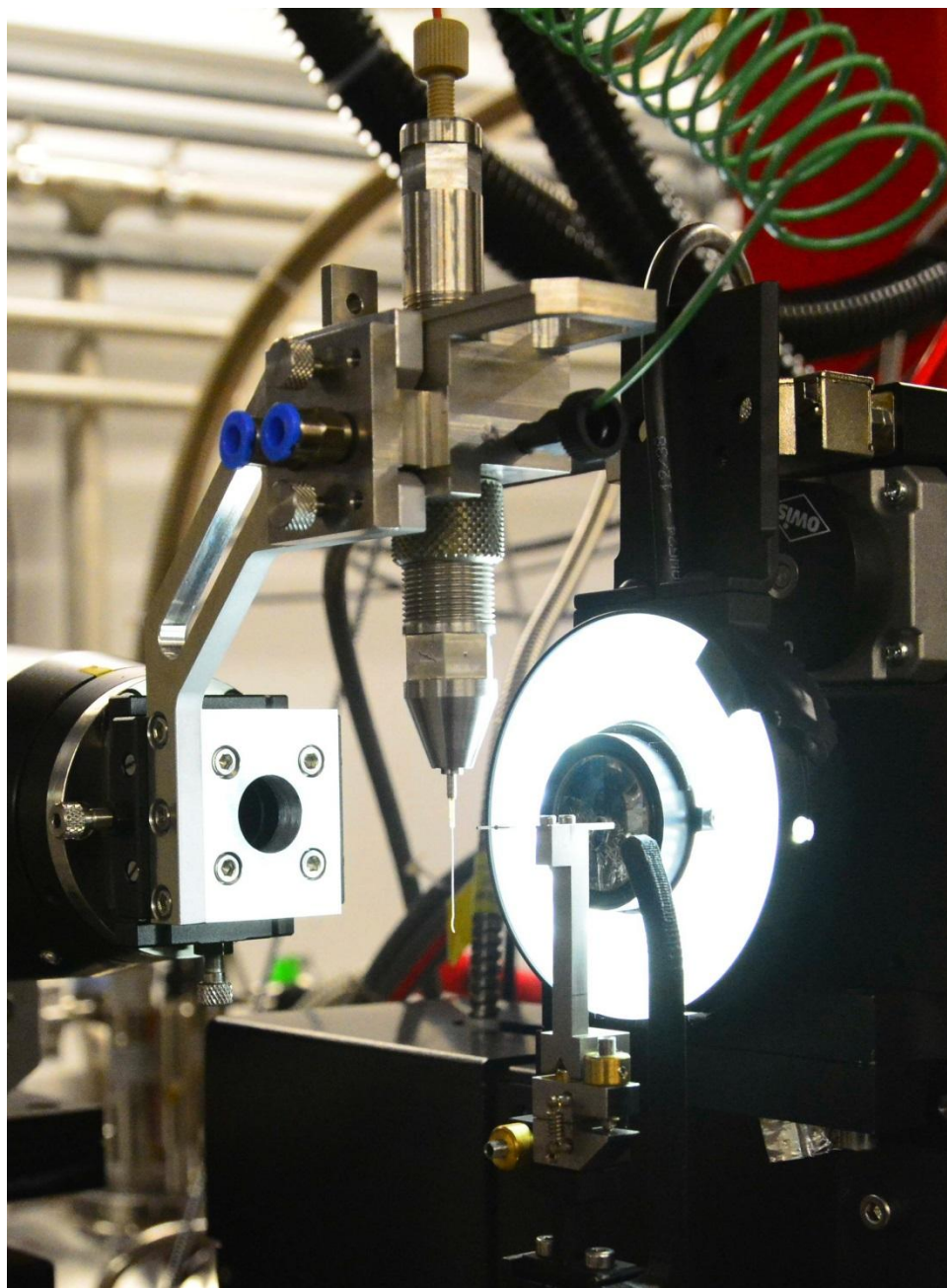
References

Barends, T. R. M., Foucar, L., Botha, S., Doak, R. B., Shoeman, R. L., Nass, K., Koglin, J. E., Williams, G. J., Boutet, S., Messerschmidt, M. & Schlichting, I. (2014). *Nature* **505**, 244-247.

Boutet, S., Lomb, L., Williams, G. J., Barends, T. R. M., Aquila, A., Doak, R. B., Weierstall, U., DePonte, D. P., Steinbrener, J., Shoeman, R. L., Messerschmidt, M., Barty, A., White, T. A., Kassemeyer, S., Kirian, R. A., Seibert, M. M., Montanez, P. A., Kenney, C., Herbst, R., Hart, P., Pines, J., Haller, G., Gruner, S. M., Philipp, H. T., Tate, M. W., Hromalik, M., Koerner, L. J., van Bakel, N., Morse, J., Ghonsalves, W., Arnlund, D., Bogan, M. J., Caleman, C., Fromme, R., Hampton, C. Y., Hunter, M. S., Johansson, L. C., Katona, G., Kupitz, C., Liang, M., Martin, A. V., Nass, K., Redecke, L., Stellato, F., Timneanu, N., Wang, D., Zatsepin, N. A., Schafer, D., Defever, J., Neutze, R., Fromme, P., Spence, J. C. H., Chapman, H. N. & Schlichting, I. (2012). *Science* **337**, 362-364.

Stellato, F., Oberthur, D., Liang, M., Bean, R., Gati, C., Yefanov, O., Barty, A., Burkhardt, A., Fischer, P., Galli, L., Kirian, R. A., Meyer, J., Panneerselvam, S., Yoon, C. H., Chervinskii, F., Speller, E., White, T. A., Betzel, C., Meents, A. & Chapman, H. N. (2014). *IUCrJ* **1**, 204-212.

Weierstall, U., James, D., Wang, C., White, T. A., Wang, D., Liu, W., Spence, J. C. H., Doak, R. B., Nelson, G., Fromme, P., Fromme, R., Grotjohann, I., Kupitz, C., Zatsepin, N. A., Liu, H., Basu, S., Wacker, D., Han, G. W., Katritch, V., Boutet, S., Messerschmidt, M., Williams, G. J., Koglin, J. E., Seibert, M. M., Klinker, M., Gati, C., Shoeman, R. L., Barty, A., Chapman, H. N., Kirian, R. A., Beyerlein, K. R., Stevens, R. C., Li, D., Shah, S. T. A., Howe, N., Caffrey, M. & Cherezov, V. (2014). *Nature Communications* **5**.

Weierstall, U., Spence, J. C. H. & Doak, R. B. (2012). *Review of Scientific Instruments* **83**.

Weiss, M. S. (2001). *Journal of Applied Crystallography* **34**, 130-135.

Weiss, M. S., Sicker, T. & Hilgenfeld, R. (2001). *Structure* **9**, 771-777.

Zeldin, O. B., Gerstel, M. & Garman, E. F. (2013). *Journal of Applied Crystallography* **46**, 1225-1230.